NMR Dynamics-Derived Insights into the Binding Properties of a Peptide Interacting with an SH2 Domain†

Patrick J. Finerty, Jr.,‡,§ Anthony K. Mittermaier,‡,§ Ranjith Muhandiram,|| Lewis E. Kay,§,||,⊥ and Julie D. Forman-Kay*,‡,§

Structural Biology and Biochemistry, The Hospital for Sick Children, 555 University Avenue, Toronto, Ontario, Canada M5G 1X8, Department of Biochemistry, University of Toronto, Toronto, Ontario, Canada M5S 1A8, Department of Medical Genetics and Microbiology, University of Toronto, Toronto, Ontario, Canada M5S 1A8, and Department of Chemistry, University of Toronto, Toronto, Ontario, Canada M5S 1A8

Received June 29, 2004; Revised Manuscript Received October 6, 2004

ABSTRACT: The signal transduction protein phospholipase C-γ1 (PLC-γ1) is activated when its C-terminal SH2 domain (PLCC) binds the phosphorylated Tyr-1021 site (pTyr-1021) in the β-platelet-derived growth factor receptor (PDGFR). To better understand the contributions that dynamics make to binding, we have used NMR relaxation experiments to investigate the motional properties of backbone amide and side chain methyl groups in a peptide derived from the pTyr-1021 site of PDGFR, both free and in complex with the PLCC SH2 domain. The free peptide has relaxation properties that are typical for a small, unstructured polymer, while the backbone of the bound peptide is least flexible for residues in the central portion of the binding site with the amplitude of pico- to nanosecond time scale motions increasing toward the C-terminus of the peptide. The increase in large amplitude motion toward the end of the pY1021 peptide is consistent with the bound peptide existing as an ensemble of states with C-terminal residues having the broadest distribution of backbone conformations, while residues in the central binding site are the most restricted. Deuterium spin relaxation experiments establish that the protein−peptide interface is highly dynamic, and this mobility may play an important role in modulating the affinity of the interaction.

Protein−protein interactions play an integral role in the regulation of cellular processes. Many of these interactions involve small modular binding domains, independently folding sequences that occur in a variety of proteins and mediate intermolecular contacts. For example, the members of the SH2 class of modular binding domains are ~100 amino acids in length and generally recognize phosphotyrosine-containing sites in their target proteins. Binding can affect the subcellular localization of both SH2 domain-containing proteins and their targets, bringing enzymes and their substrates into proximity. Phospholipase C-γ1 (PLC-γ1)[1] is activated when its C-terminal SH2 domain (PLCC) binds the pTyr-1021 site in the β-platelet-derived growth factor receptor (PDGFR), leading to phosphorylation by the receptor tyrosine kinase (*1*, *2*). Activated PLC-γ1 catalyzes the hydrolysis of phosphatidylinositol 4,5-bisphosphate to diacylglycerol and inositol 1,4,5-triphosphate, two second messengers involved in the activation of protein kinase C and in the release of Ca^{2+} from internal cellular stores, respectively (*3*).

Tertiary structures have been determined for several SH2 domains in complex with various peptides (*4*−*7*), including the PLCC SH2 domain in complex with a peptide derived from the pTyr-1021 site of PDGFR [pY1021 (*8*)]. The PLCC SH2 domain recognizes the consensus pTyr-hydrophobic-X-hydrophobic sequence (*9*) with the pTyr bound in a deep pocket and residues C-terminal to the pTyr lying in an extended hydrophobic groove (Figure 1a). Residues in the hydrophobic binding groove of the PLCC SH2 domain make extensive contacts with the bound peptide (Figure 1b), yet it has been shown that the pY1021 peptide can be truncated to the +1 position (relative to the pTyr, residue I5 in the pY1021 peptide) with only a modest reduction in binding affinity, despite the fact that numerous NOEs were observed between the PLCC SH2 domain and residues following I5 in the peptide (Figure 1b) (*10*).

To investigate why interactions that are evident in the NMR structure do not contribute significantly to binding affinity, the free and bound states of the PLCC SH2 domain were further characterized using NMR relaxation experiments that probe rapid picosecond to nanosecond time scale dynamics of backbone amide and side chain methyl groups (*10*−*13*). Interestingly, deuterium-based NMR experiments establish that side chain methyls in the hydrophobic groove of the PLCC SH2 domain have significant motional disorder

† This research was supported by the National Cancer Institute of Canada with funds from the Canadian Cancer Society and by the Ontario Premier's Research Excellence Award program. L.E.K. holds a Canada Research Chair in Biochemistry.

* To whom correspondence should be addressed. Phone: (416) 813-5358. Fax: (416) 813-5022. E-mail: forman@sickkids.ca.

‡ The Hospital for Sick Children.

§ Department of Biochemistry, University of Toronto.

|| Department of Medical Genetics and Microbiology, University of Toronto.

⊥ Department of Chemistry, University of Toronto.

[1] Abbreviations: SH2, Src homology 2; PLCC, C-terminal SH2 domain of phospholipase C-γ1; PDGFR, β-platelet-derived growth factor receptor; pTyr, phosphotyrosine; pY1021, phosphopeptide derived from the pTyr-1021 site of PDGFR; NOE, nuclear Overhauser enhancement.

10.1021/bi048641k CCC: $30.25
Published on Web 12/16/2004

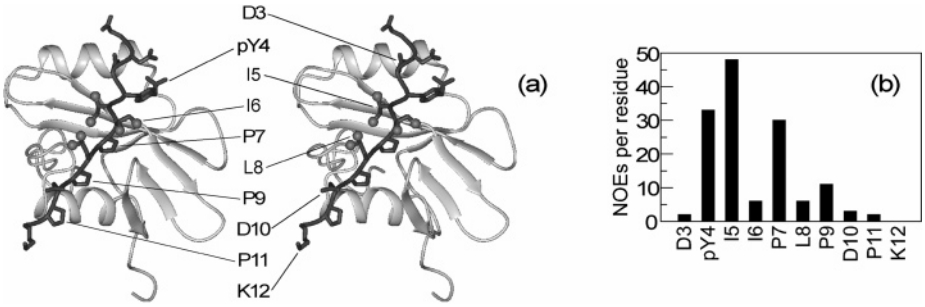

FIGURE 1: (a) Stereo backbone ribbon diagram of the refined solution structure of the PLCC SH2 domain complexed with a phosphorylated peptide derived from the pTyr-1021 site of PDGFR (*8*). The pY1021 peptide is colored dark gray, with methyl groups from the peptide shown as spheres. This illustration was produced using MOLMOL (*52*). (b) Number of intermolecular NOE contacts with the PLCC SH2 domain as a function of peptide residue number (*53*). Resonances for the two N-terminal residues of the free and bound states of the peptide were not visible in $^{1}H-^{15}N$ spectra and so are absent from this and subsequent plots. All plots were produced using Grace (http://plasma-gate.weizmann.ac.il/Grace).

that is not reduced upon peptide binding. Since van der Waals interactions are strongly distance-dependent, this disorder may explain why many of the protein−ligand interactions do not contribute significant binding energy (*10*).

As illustrated by the results presented above, even though the tertiary structures of many SH2 domain−peptide complexes have been determined, it is currently not possible to identify affinity- or specificity-determining residues based exclusively on "static" structural data. Consequently, there has been much interest in obtaining site-specific dynamics information in an effort to better understand the atomic-level interactions that govern the stability of protein complexes. NMR dynamics experiments performed on a variety of systems have yielded information about the effect of ligand binding on motional properties of the protein backbone as well as side chain methyl groups (*10*, *12*, *14*−*23*). For some proteins, ligand binding leads to a reduction in fast time scale dynamics (*14*, *21*, *22*, *24*), while in other instances, the overall flexibility of the backbone can remain unchanged or even increase (*11*, *18*, *19*, *22*). In many cases, these studies provide insights into the thermodynamics of binding.

The NMR experiments performed on the PLCC SH2 domain complexed with the pY1021 peptide, as well as similar studies on related systems, have provided useful information about the changes in protein dynamics that occur upon ligand binding. However, data for the other half of the complex, namely, the peptide, have been lacking. To obtain information complementary to that previously measured for the PLCC SH2 domain, we have measured ^{15}N and ^{2}H NMR relaxation parameters for the free and bound states of uniformly ^{15}N- and ^{13}C-labeled and randomly fractionally ^{2}H-labeled pY1021 peptide.

MATERIALS AND METHODS

Expression, Purification, and Preparation of ^{15}N, ^{13}C, $^{2}H(50\%)$ pY1021 Peptide. Oligonucleotides encoding Y1021, a 12-residue peptide derived from the sequence surrounding Tyr-1021 of the PDGFR (DNDYIIPLPDPK), were cloned into the plasmid pMMHb (*25*), provided by the laboratory of P. S. Kim, to make the pMMHb-Y1021 plasmid. Purification of proteins expressed using the pMMHb plasmid has been described previously (*25*). Briefly, following expression of the Y1021 peptide as a fusion with a modified form of the TrpLE leader sequence, the insoluble fusion protein was purified by Ni^{2+} affinity chromatography under denaturing conditions and the peptide subsequently cleaved from the purified fusion protein using CNBr. For NMR relaxation experiments, the Y1021 peptide was expressed in *Escherichia coli* strain BL21(DE3) cells grown in 2 L of M9 minimal medium (50% D_2O/50% H_2O) with $^{15}NH_4Cl$ and [^{13}C]-glucose as the sole nitrogen and carbon sources, respectively. After CNBr cleavage, the Y1021 peptide was further purified by reverse phase HPLC on a semipreparative C18 column (Beckman) prior to phosphorylation.

The Y1021 peptide was phosphorylated using the cytoplasmic domain of the EphA4 receptor protein tyrosine kinase ($EphA4_{CYTO}$). Plasmid DNA for bacterial expression of $EphA4_{CYTO}$ was kindly provided by the laboratory of T. Pawson; the expression and purification protocol for this protein has been described elsewhere (*26*). The kinase reaction, employing $EphA4_{CYTO}$ prepared from a 2 L LB culture, was performed at 30 °C in a buffer containing 10 mM HEPES (pH 7.5), 10 mM $MgCl_2$, 1.5 mM dATP, and 0.6 mM Y1021 peptide and the progress of the reaction monitored by HPLC. Following completion of the reaction (∼90% phosphorylation of Y1021, ∼3 h), separation of the phosphorylated peptide from the kinase and nonphosphorylated peptide was accomplished using reverse phase HPLC on a semipreparative C18 column (Beckman), and the purity and integrity of the phosphorylated peptide were confirmed by mass spectrometry.

Preparation of NMR Samples. Assignment of backbone and side chain resonances for the unbound peptide was performed using a sample of 1.6 mM ^{15}N, ^{13}C, $^{2}H(50\%)$ pY1021 peptide in pY1021 NMR buffer [100 mM $NaHPO_4$ (pH 6.0) and 100 μM EDTA] with a 90% H_2O/10% D_2O mixture. Uniformly ^{15}N-labeled and unlabeled PLCC SH2 domain were prepared as described previously (*8*) and dialyzed into PLCC NMR buffer (pY1021 NMR buffer with 100 μM DTT). The PLCC SH2 domain complex with the pY1021 peptide was prepared by adding uniformly ^{15}N-labeled PLCC SH2 domain in PLCC NMR buffer with a 90% H_2O/10% D_2O mixture to uniformly labeled ^{15}N, ^{13}C, $^{2}H(50\%)$ peptide in pY1021 NMR buffer. However, to completely eliminate resonances from unbound pY1021 peptide, a small amount of unlabeled PLCC SH2 domain in PLCC NMR buffer with a 90% H_2O/10% D_2O mixture was added to the sample to yield an excess (<10% molar excess) of SH2 domain relative to the peptide (^{15}N-labeled PLCC SH2 domain not available at the time). Following the

titration, the sample was equilibrated with PLCC NMR buffer through four rounds of concentration and dilution in a Centriprep YM10 ultrafiltration concentrator (Amicon). Relaxation dispersion experiments (see below) utilized a similarly prepared sample containing uniformly ^{15}N-labeled pY1021 peptide (prepared as for the triple-labeled sample) in complex with unlabeled PLCC SH2 domain. The concentration of the complex, determined by measuring the absorbance at 280 nm and using a theoretical extinction coefficient of 14 417.1 M^{-1} cm^{-1}, was adjusted to 1 mM. All NMR samples were blanketed with argon to prevent oxidation of Cys residues.

NMR Experiments. All NMR experiments were performed at 30 °C on Varian Inova 500, 600, or 800 MHz spectrometers with triple-resonance, pulsed-field gradient probes with an actively shielded *z* gradient coil. ^{1}HN, ^{15}N, ^{13}Cα, ^{13}Cβ, ^{13}C-carbonyl, and side chain ^{13}C-methyl assignments for the free pY1021 peptide were obtained from CBCA(CO)NH, HNCACB, HNCO, (H)CC(CO)NH-TOCSY, H(CC)(CO)-NH-TOCSY, HACAN, and homonuclear NOESY spectra recorded using enhanced sensitivity pulsed-field gradient methodology (*27*−*29*). Peptide proton assignments of bound pY1021 peptide were reported previously (*8*), and these were used to guide assignment of ^{15}N- and ^{13}C-methyl resonances of the pY1021 peptide in spectra of the complex with the PLCC SH2 domain. ^{13}C-methyl chemical shifts for the peptide were confirmed with an (H)CC(CO)NH-TOCSY experiment. The two Leu methyl groups in free pY1021 were stereoassigned using published chemical shift values (*30*), and the same assignments were used for the complexed peptide, as the chemical shifts of these groups are very similar in the free and bound states. Assignments were made using the Linux version of NMRView (*31*).

^{15}N Relaxation Experiments. ^{15}N R_1, $R_{1\rho}$, and NOE values were measured at 600 MHz using previously published pulse schemes (*11*, *32*) that were modified to separate ^{1}H−^{15}N correlations for which the ^{15}N nuclei are bonded to ^{13}C nuclei (in the case of the pY1021 peptide) from those that are not (in the case of the PLCC SH2 domain). Steady-state NOE values for free pY1021 (PLCC SH2 domain-pY1021 complex) were obtained from ^{1}H−^{15}N correlation spectra with saturation of ^{1}H for 5 (5) s and a 10 (7) s delay between scans and without ^{1}H saturation using a 15 (12) s delay between scans. ^{15}N R_1 values were measured from spectra recorded with seven different values of the relaxation delay (10.1, 90.8, 201.7, 322.7, 463.9, 645.4, and 857.1 ms and 10.1, 70.6, 151.2, 252, 352.8, 493.9, and 655.2 ms for free pY1021 and complexed pY1021, respectively). ^{15}N $R_{1\rho}$ values were measured from spectra recorded with delays of 10, 30, 50, 70, 90, 110, 130, and 150 ms and 10, 20, 30, 40, 60, 80, and 100 ms for free pY1021 and complexed pY1021, respectively. ^{15}N R_2 values for each residue were obtained by correction of the observed relaxation rate $R_{1\rho}$ for the offset $\Delta\nu$ of the applied spin-lock rf field (ν_1) to the resonance using the relation $R_{1\rho} = R_1 \cos^2\theta + R_2 \sin^2\theta$, where $\theta = \tan^{-1}(\nu_1/\Delta\nu)$. ν_1 was 1041.7 and 1582.3 Hz for free pY1021 and the PLCC SH2 domain-pY1021 complex, respectively. ^{15}N relaxation dispersion experiments with the pY1021 peptide bound to the PLCC SH2 domain, conducted at 500 and 800 MHz, were performed and analyzed as described previously (*33*) with spectral widths of 8000.0 and 1500.0 Hz (at 500 MHz, recorded as a 100 × 576 complex matrix) and 12 775.5 and 2400 Hz (at 800 MHz, recorded as a 112 × 826 complex matrix) employed in the ^{1}H and ^{15}N dimensions, respectively. Spectra for the free peptide (PLCC SH2 domain-pY1021 complex) were recorded as 64 × 576 (100 × 576) complex matrices with spectral widths of 9000.9 (9000.9) and 750 (1800) Hz employed in the ^{1}H and ^{15}N dimensions, respectively. All data sets were processed using the Linux version of the NMRPipe suite (*34*) with Lorentzian-to-Gaussian apodization in both dimensions.

Peak intensities were obtained using the Linux version of NMRView (*31*) and relaxation times generated from a fit to a two-parameter function of the form $I(t) = I_0 e^{-tR1,2}$ with a MATLAB script written in house. Errors in relaxation rates were estimated by Monte Carlo analysis. Steady-state NOE values were determined from the ratios of peak heights with and without proton saturation using NMRView. Errors in peak heights were estimated from the root-mean-square value of background noise in the spectra.

Analysis of Relaxation Parameters for the PLCC SH2 Domain-pY1021 Complex. ^{15}N R_1 and $R_{1\rho}$ rates for the ^{15}N, ^{13}C, ^{2}H(50%) pY1021 peptide and the ^{15}N-labeled PLCC SH2 domain were measured simultaneously (see above) using experiments which either selected for (peptide) or against (SH2 domain) ^{15}N spins one-bond coupled to ^{13}CO. Spectra were recorded in an interleaved manner and separated using software written in house and processed with NMRPipe (*34*). In a previous study, values of 9.2 and 6.6 ns were obtained for the rotational correlation times of the free and pY1021-complexed SH2 domains, respectively, indicating that the free protein has a tendency to self-associate (*11*), a property that has also been noted for other SH2 domains (*14*, *21*, *35*). While past NMR relaxation experiments with the complexed state of the PLCC SH2 domain employed samples containing an excess of peptide, in this study we utilized a complementary strategy in which excess SH2 domain was present to maximize the fraction of bound peptide.

The presence of a slight excess of SH2 domain (and hence a small degree of free protein that can self-associate) complicates the extraction of accurate correlation times from fits of relaxation data. This is particularly the case since very few ^{1}H−^{15}N cross-peaks shift upon binding of the peptide so that it is not possible to obtain a sufficient number of unique correlations representing the bound form of the protein. Data from the pY1021 peptide amide resonances would not provide a reliable correlation time since, with only seven resonances, there are not enough orientations of bond vectors and some are affected by intermediate time scale motion. We have therefore used a τ_c value of 6.6 ns from previous studies and calculated the orientation of the diffusion tensor with relaxation data recorded on the complex with a slight excess of protein. The analysis was performed with the quadric_diffusion program provided by the Palmer laboratory (http://cpmcnet.columbia.edu/dept/gsas/biochem/labs/palmer/software.html). Residues with NOE ratios of <0.7 were excluded from the input data set. An axially symmetric rotational diffusion tensor ($D_{||}/D_{\perp} = 1.13$) was found to offer a slightly better fit of the data over the fully isotropic model, while the anisotropic model did not significantly improve the fit (*P* values obtained from a comparison of the axially symmetric and isotropic models and the axially symmetric and anisotropic models were 0.006

and 0.55, respectively). Simulations have established that very small errors are introduced by neglecting anisotropy (less than 1% change in ^{15}N S^2 values, on average, with the largest change being <1.5%; 2.3% change in the ^{2}H order parameters, on average, with the largest change being <4%), and all of the data has been analyzed therefore with a single value of τ_c.

The pY1021 peptide used for measurement of ^{15}N relaxation parameters in the free and bound states was uniformly labeled with ^{15}N and ^{13}C; however, effects due to dipolar relaxation via ^{13}Cα and ^{13}CO spins were not included in our calculations. We calculate that these pathways would lead to a nearly homogeneous error in the ^{15}N S^2 values presented here of <3%.

^{2}H Relaxation Experiments. ^{2}H NMR relaxation experiments measuring the decay of the spin-operator terms D_z, D_+, $3D_z^2 - 2$, $D_+D_z + D_zD_+$, and D_+^2 were recorded at a spectrometer field of 600 MHz using previously described pulse schemes (*12*, *36*). The relaxation rate of the D_+^2 spin-operator term was not measured for the free peptide. D_z rates were obtained from two-dimensional ^{1}H$-^{13}$C correlation spectra with relaxation delays of 0.05, 6.7, 14.1, 22.7, 32.7, 44.7, and 60 ms for both the free peptide and the SH2 domain pY1021 complex, while D_+ rates were measured with relaxation delays of 1.1, 5.6, 11.8, 18.9, 27.2, 37.2, and 50 ms and 0.2, 4.2, 6.6, 9.4, 12.6, 16.4, and 21 ms for the free peptide and the SH2 domain-pY1021 complex, respectively. The decay rates for quadrupolar order and double-quantum coherences were obtained with delay values very similar to those used for D_z, while delays used to record the decay of $D_+D_z + D_zD_+$ were similar to those used for measurement of the relaxation of D_+. All spectra were recorded as 102 × 576 complex matrices with spectral widths of 9000.9 and 3600 Hz employed in the ^{1}H and ^{13}C dimensions, respectively. Processing and analysis of spectra were as described previously (*13*).

RESULTS

Sample Preparation and Chemical Shift Assignments. The pY1021 peptide (DNDpYIIPLPDPK, where pY represents phosphotyrosine) used in NMR experiments was uniformly labeled with ^{15}N and ^{13}C and randomly fractionally deuterated to approximately 50% as described in Materials and Methods. A single preparation was used for all experiments. The PLCC SH2 domain was labeled with ^{15}N. Samples of the pY1021 peptide complexed with the PLCC SH2 domain contained an excess of the SH2 domain (less than 10% molar excess) to ensure the absence of the free peptide. ^{15}N and ^{2}H NMR relaxation experiments were performed on the same samples except for relaxation dispersion experiments, which utilized a sample of the ^{15}N-labeled peptide in complex with the unlabeled PLCC SH2 domain.

Backbone amide and methyl resonances of the peptide were assigned as described in Materials and Methods. Assignments of the bound state of the PLCC SH2 domain and ^{1}H assignments of the pY1021 peptide bound to the PLCC SH2 domain were reported previously (*8*). Resonances for the two N-terminal residues of both the free and bound states of the peptide were not visible in ^{1}H$-^{15}$N spectra, likely due to rapid exchange with the solvent. The pY1021 peptide contains three proline residues C-terminal to the pTyr, and ^{1}H$-^{15}$N spectra of the free peptide showed several weak peaks, indicating the presence of various combinations of proline isomers (data not shown), although only the peaks of the major conformer were unambiguously assigned. In addition to those peaks resulting from the major species, a number of weak correlations were also present in ^{1}H$-^{15}$N spectra of the bound peptide. These likely arise from isomerization of the most C-terminal proline residue that makes only a few contacts with the SH2 domain (Figure 1b; *8*), with the other prolines stably populating *trans* peptide bond configurations. Resonances from this minor C-terminal conformer were not able to be assigned clearly due to overlap. ^{1}H$-^{13}$C correlation maps of CH_2D groups of the free and bound states showed only six resonances, corresponding to the six methyl groups in the peptide.

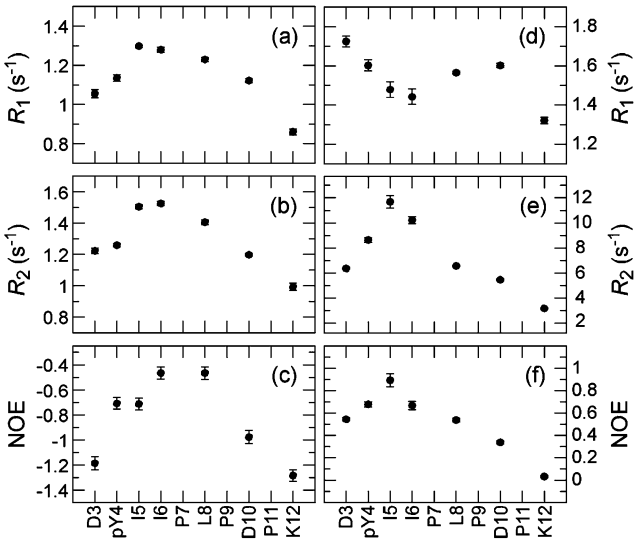

FIGURE 2: ^{15}N R_1 rates (a and d), R_2 rates (b and e), and steady-state ^{1}H$-^{15}$N NOE ratios (c and f) as a function of residue number for the free pY1021 peptide (a−c) and for the peptide in complex with the PLCC SH2 domain (d−f) with error bars indicating the uncertainties in the measurements.

NMR Relaxation Experiments. Backbone ^{15}N spin relaxation experiments (*11*) were conducted at 600 MHz and 30 °C and analyzed as described in Materials and Methods, yielding R_1, R_2, and steady-state ^{1}H$-^{15}$N NOE values. ^{15}N relaxation data for seven residues (from the dominant species; see above) were obtained for the free and bound peptide, and these values are plotted in Figure 2. The R_1 and R_2 rates measured for the free peptide are generally similar for a given residue. This is not the case for the bound state, with the exception of K12, the most C-terminal position. Interestingly, only residues pY4, I5, and I6 exhibit R_1 and R_2 rates that are comparable to those measured for residues in the SH2 domain (data not shown; *11*), suggesting that the peptide backbone is least dynamic in this region. Steady-state ^{1}H$-^{15}$N NOE values are negative for the free peptide, as expected, but positive for the bound state, with the exception again of that of residue K12 (NOE ratio ≈ 0, Figure 2f).

Side chain ^{2}H $R^Q(D_z)$, $R^Q(D_+)$, $R^Q(3D_z^2 - 2)$, $R^Q(D_+D_z + D_zD_+)$, and $R^Q(D_+^2)$ relaxation parameters were measured for CH_2D methyl groups at 600 MHz and 30 °C [relaxation of double-quantum coherence, $R^Q(D_+^2)$, was not measured for the free peptide] and analyzed according to published procedures (*10*, *12*, *13*, *36*, *37*; see Materials and Methods). The nomenclature used here for the ^{2}H rates is the same as

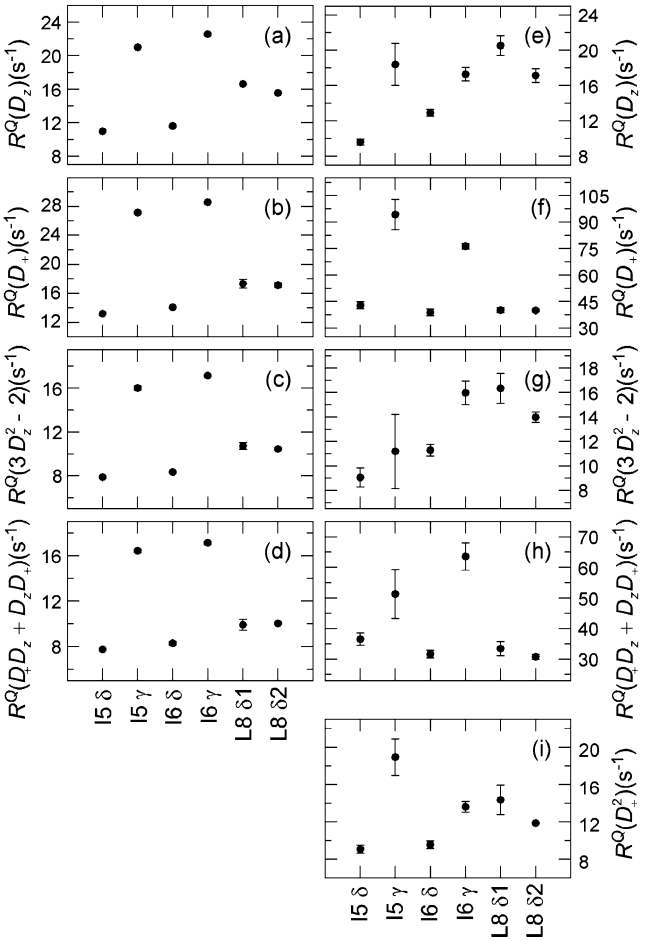

FIGURE 3: ^{2}H spin relaxation rates as a function of residue number for the free pY1021 peptide (a−d) and for the peptide in complex with the PLCC SH2 domain (e−i) with error bars showing the uncertainties in the measurements. The double-quantum coherence relaxation rate was not measured for the free peptide.

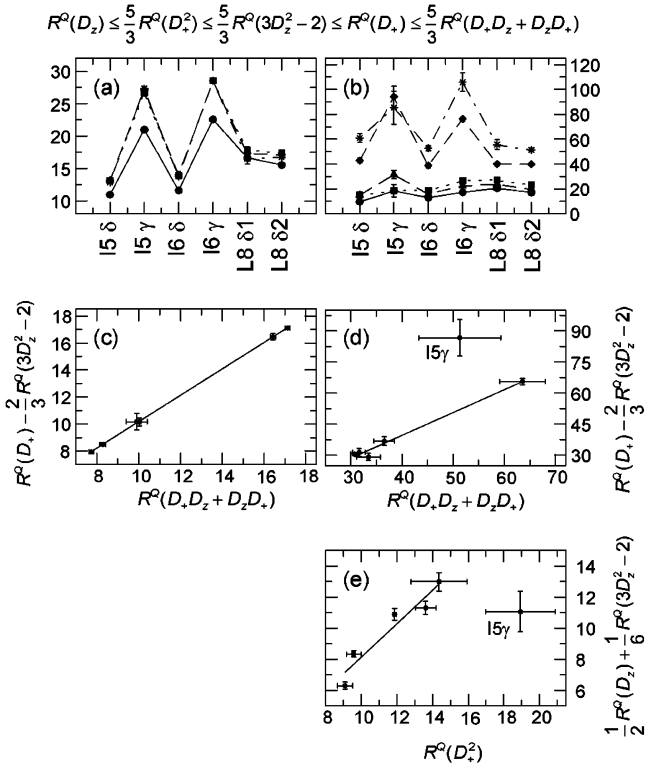

FIGURE 4: Inequality $R^Q(D_z) \le {}^5/_3R^Q(D_+^2) \le {}^5/_3R^Q(3D_z^2 - 2) \le R^Q(D_+) \le {}^5/_3R^Q(D_+D_z + D_zD_+)$ (a and b) and consistency relationships $R^Q(D_+D_z + D_zD_+) = R^Q(D_+) - {}^2/_3R^Q(3D_z^2 - 2)$ (c and d) and $R^Q(D_+^2) = {}^1/_2R^Q(D_z) + {}^1/_6R^Q(3D_z^2 - 2)$ (e) evaluated using the experimentally measured ^{2}H quadrupolar relaxation rates shown for the free pY1021 peptide (a and c) and the complex with the PLCC SH2 domain (b, d, and e). The rates (a and b) are depicted as follows: $R^Q(D_z)$ (● and —), $R^Q(D_+)$ (◆ and − − −), ${}^5/_3R^Q(3D_z^2 - 2)$ (■ and - - -), ${}^5/_3R^Q(D_+D_z + D_zD_+)$ (* and · − ·), and ${}^5/_3R^Q(D_+^2)$ (▲ and − − −). Best fit lines are also given (c−e).

in recently published work (*36*, *37*). ^{2}H relaxation rates were obtained for all six methyl groups in the free and bound forms of the peptide and are plotted in Figure 3. Rates measured for the free peptide are very similar for each methyl type and show little variation among the four experiments. In contrast, ^{2}H rates measured for the bound pY1021 peptide show a broad distribution of values (particularly the rates that measure the decay of transverse magnetization), indicating that the dynamics of the various methyl groups are diverse. While resonances for the bound state are not as intense as those obtained for the free peptide, the resonance for one methyl group in particular, I5 Cγ2, is very weak (approximately one-third as intense as that of the I6 Cγ2 methyl group, data not shown), likely due to intermediate time scale motion that affects the efficiency of ^{13}C−^{2}H magnetization transfer. The poor signal for the I5 Cγ2 methyl group results in significantly larger errors in the ^{2}H relaxation rates compared to those obtained for the other methyls.

Previously, it has been shown that the five different quadrupolar relaxation rates measured here must fulfill the following inequalities: $R^Q(D_z) \le {}^5/_3R^Q(D_+^2) \le {}^5/_3R^Q(3D_z^2 - 2) \le R^Q(D_+) \le {}^5/_3R^Q(D_+D_z + D_zD_+)$ so long as $J(0) \ge J(\omega_D) \ge J(2\omega_D)$ (*38*). Additionally, ^{2}H relaxation rates can be related by a pair of consistency relationships: $R^Q(D_+D_z + D_zD_+) = R^Q(D_+) - {}^2/_3R^Q(3D_z^2 - 2)$ and $R^Q(D_+^2) = {}^1/_2R^Q(D_z) + {}^1/_6R^Q(3D_z^2 - 2)$ (*38*). Millet et al. noted that the equations given above were completely satisfied for all five ^{2}H relaxation rates measured on protein L (*36*). The ^{2}H rates for the free and bound states of the pY1021 peptide are given in Figure 4. Since the ^{2}H relaxation rates for the free peptide were not used to calculate order parameters (see below), the primary goals of qualitative analysis of the trends and testing their consistency were met by measuring only four rates. Rates for all methyl groups in the free peptide satisfy the inequalities given above (Figure 4a) as well as the first consistency relation [Figure 4c; note that $R^Q(D_+^2)$ rates were not measured so that the second relation could not be verified], while data for one methyl group in the bound state, I5 Cγ2, fail the validation tests (Figure 4b,d,e). It is likely that the weak signal for this methyl group prevents measurement of reliable relaxation rates for D_+^2, $3D_z^2 - 2$, or $D_+D_z + D_zD_+$ since the experiments that are used for these elements are less sensitive than those used to measure the $R^Q(D_z)$ and $R^Q(D_+)$ rates. In what follows, only the longitudinal and in-phase transverse relaxation rates are analyzed further for I5 Cγ2 in the bound state.

Analysis of Relaxation Data for the Free Peptide. Amide ^{15}N relaxation rates and steady-state ^{1}H−^{15}N NOE ratios for the free peptide show a broad range of values that are largest in the center and decrease closer to the ends, a pattern that is characteristic of a small polymer with unrestrained ends. Simulations performed by other groups have shown that large amplitude motions occurring on short time scales are

prevalent near the ends of theoretical polymer chains on a tetrahedral lattice (*39*). Still, the pY1021 peptide does not behave completely like a homogeneous polymer as evidenced by variations in the relaxation rates and steady-state ^{1}H−^{15}N NOE ratios along the chain. Some of this variability is likely caused by the conformational restrictions imposed by the three proline residues in the C-terminal half of the peptide. The variability in the N-terminal half of the pY1021 peptide may be due to local interactions, although amide ^{1}H chemical shifts for the free state (data not shown) are very close to random coil values, indicating that the peptide likely has little structure. Furthermore, each of the three different methyl types in the free pY1021 peptide (Ile Cγ2, Ile Cδ1, and Leu Cδ methyl groups) has a similar relaxation rate (Figure 3a−d), also suggesting little persistence of local interactions within the peptide at the level of these hydrophobic side chains.

Analysis of Relaxation Data for the Bound Peptide. To facilitate comparisons of fast time scale dynamics in proteins, it is useful to employ the model-free (*40*, *41*) analysis in which an order parameter (S^2) and effective correlation time for internal motions (τ_e) are calculated. Order parameters describe the amplitude of internal pico- to nanosecond time scale motions for a particular bond vector and range from 0, for a vector rapidly sampling an isotropic distribution of orientations, to 1, for no internal motion. For methyl dynamics, S_{axis}^2 describes the amplitude of pico- to nanosecond motions for the bond vector between the methyl carbon and its directly attached carbon atom. Note that ^{15}N and ^{2}H relaxation data measured for the free pY1021 peptide (Figures 2a−c and 3a−d) were not analyzed using the model-free formalism. Because of its small size (12 residues) and the relatively high temperature at which the relaxation experiments were performed (30 °C), the peptide is unstructured, and it would be difficult to quantify the dynamics using any simple model of motion. Moreover, separation of internal from overall dynamics is problematic for a small peptide of this size [a very qualitative estimate of the rotational correlation time from ^{15}N R_1/R_2 ratios (*42*) is on the order of ~0.7 ns].

^{15}N and ^{2}H relaxation data measured for the pY1021 peptide bound to the PLCC SH2 domain were used to calculate order parameters with MATLAB scripts written in house. ^{15}N relaxation data have been analyzed using a three-parameter model (S^2, τ_e, and R_{ex}) that takes into account contributions to transverse relaxation from exchange between sites (*43*). A single overall rotational correlation time [6.6 ns (*11*)] was used for all residues of the peptide; the anisotropy of the diffusion tensor for the complex is small ($D_{||}/D_{\perp} = 1.13$), and order parameters fit using isotropic versus axially symmetric tumbling models differ by less than 2.5%, on average. In contrast, ^{2}H rates were interpreted in terms of a model in which S^2 and τ_e are fitting parameters. As described previously (*12*, *36*), the deuterium relaxation rates are dominated by the quadrupolar interaction and the effects of chemical exchange can be neglected. *F* test analyses have established that more complex motional models do not yield statistically significant improvements in fits of the data. Calculated ^{15}N and ^{2}H order parameters are plotted in Figure 5. As described above, only the $R^Q(D_z)$ and $R^Q(D_+)$ rates have been analyzed for I5 Cγ2.

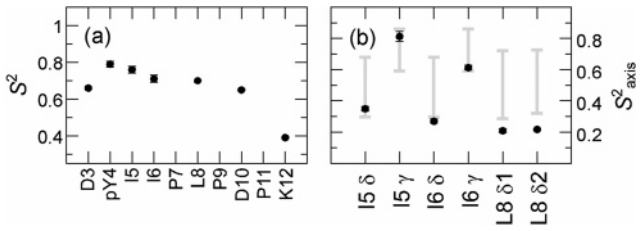

FIGURE 5: Backbone amide (a) and methyl axis order parameters squared (b) as a function of residue number (●) for the bound state of the pY1021 peptide with error bars (black lines) indicating the uncertainty in the calculated order parameters. In panel b, thick gray lines show the distribution of database values for methyl axis order parameters (±1 standard deviation) (*23*). Note that in panel b the S^2_{axis} value for I5 Cγ2 was calculated using only the ^{2}H R_1 and $R_{1\rho}$ relaxation rates.

Amide ^{15}N Dynamics in the Bound Peptide. The structural, dynamic, and binding properties of the PLCC SH2 domain have been extensively characterized in previous work by our group (*8*, *10*, *11*, *13*), providing the opportunity to compare measurements reported here for the pY1021 peptide with these data. The solution structure of the PLCC SH2 domain in complex with the pY1021 peptide (Figure 1a) establishes that the protein interacts with peptide residues C-terminal to the pTyr via an extended hydrophobic groove and that NOEs from three peptide residues, pY4, I5, and P7, account for more than 75% of the total protein−peptide distance restraints (Figure 1b; *8*). Subsequent binding studies using peptide ligands that were progressively truncated demonstrated that the SH2 domain bound the ligand Ac-D-pY-I-NH_2 with an only 15-fold reduction in affinity compared to the 12-mer peptide used for structural and dynamics experiments.

^{15}N order parameters determined for the bound peptide (Figure 5) indicate that the pY4 and I5 amide positions are the most restricted in the complex, as might be expected on the basis of structural (*8*; Figure 1) and binding data (*10*). Notably, the next most restricted amide position is that of I6, a residue that is not required for high-affinity binding (*10*). The absence of I6 in a peptide which binds with an only 15-fold reduction in affinity, in combination with the NOE data (Figure 1b), suggests that this residue does not make critical interactions with the SH2 domain. The restriction in the mobility of residue I6, despite the absence of interactions with the SH2 domain, may be a consequence of its environment. Of note, I6 is flanked by I5 and P7, residues with large numbers of intermolecular NOEs.

Methyl Dynamics. Main chain atoms constitute approximately one-fifth of the area at an average protein interface with the remainder comprising amino acid side chains (*44*). Thus, to understand the energetics of protein interactions, it is necessary to investigate the dynamic properties of side chain atoms at protein interfaces in addition to those of backbone atoms. Previous work by our group on the N-terminal SH2 domain from the tyrosine phosphatase Shp2 and on the SAP SH2 domain showed that methyl groups involved in interactions with the ligand can be less mobile in the bound state than in the free state (*10*, *14*). In contrast, dynamics experiments performed on the PLCC SH2 domain establish that methyls within 5 Å of positions +2 through +5 (C-terminal in relation to pY) of the pY1021 peptide are highly dynamic and exhibit motional disorder in both bound and free forms (*10*). Comparison of the dynamics

results to binding data suggests that those methyl groups having restricted motional properties in protein complexes contribute energetically to binding while those without reduced mobility contribute less to the energetics, even though they may be important for the specificity of the interaction. Given the importance of I5 to the binding energy (*10*), it is of interest to examine its dynamic properties and to compare them with other residues that have been shown to be less important for binding. This study also affords the opportunity to compare the extent of side chain mobility on peptide and protein "sides of the interface". There are many examples where shape, hydrophobic, and electrostatic complementarity plays an important role in molecular recognition. Large hydrophobic residues on one surface may embed in grooves in the partner molecule, or positively charged groups on one side may attract negatively charged moieties on the other, for example. An important issue to address in the case of the PLCC−pY1021 complex is one of dynamic complementarity; are the side chains of both the protein and peptide at the binding interface mobile?

Of the six methyl groups in the pY1021 peptide, only those from residue I5 have significant chemical shift differences between the free and bound states (see the Supporting Information). This observation is consistent with binding data showing that removal of Ile from the Ac-D-pY-I-NH_2 sequence decreases the ΔG of binding in excess of 1.7 kcal/mol and with structural data that establish that large numbers of contacts are formed between this residue and the PLCC SH2 domain (Figure 1b; *8*, *10*). The absence of methyl shift changes for I6 and L8 is consistent with the fact that only a relatively small number of intermolecular NOEs are observed between these residues and the SH2 domain. Interestingly, the S^2_{axis} value for I6 $\delta1(\gamma2)$ is 0.08 (0.2) lower than for I5 $\delta1$ ($\gamma2$). The order parameters of the δ-methyls of Leu8 are also lower than for I5 $\delta1$ (by $\sim$0.15) and lie at the lower end of a distribution determined using a database of values tabulated from studies of several proteins (±1 standard deviation, shown as thick gray lines in Figure 5b; *23*). Thus, both I6 and L8, which contribute less to the binding energy than I5, have higher levels of dynamics than I5. The correlation between increased motion and a decrease in the contribution to the energetics of binding that has been observed in connection with methyls of the PLCC SH2 domain is thus also noted for a number of methyl groups in the pY1021 peptide.

Slower Time Scale Motions. The relaxation measurements described above focus exclusively on pico- to nanosecond time scale dynamics. We have also quantified slower motions (micro- to millisecond time scale) by recording relaxation dispersion experiments (*33*, *45*; see Materials and Methods). Both I5 and I6 exhibit small contributions to relaxation from slow time scale dynamics with R_{ex} values on the order of 2 s^{-1}, while the dispersion profiles for the remaining residues are flat. A k_{ex} value of $\sim$75 s^{-1}, with a 5% population of the minor state, is obtained from a simultaneous analysis (*33*) of dispersion profiles for these two residues. Notably, since both I5 and I6 exhibit similar levels of millisecond time scale dynamics, such motion, at least at the level of the backbone of the peptide, cannot be correlated with the relative importance of these residues for binding to the SH2 domain. This R_{ex} contribution is consistent, however, with the weak resonance of I5 C$\gamma2$.

DISCUSSION

To gain an understanding of the factors that contribute to the stabilization of proteins and protein−ligand interactions, it is important to understand motions within proteins and at protein interfaces. Several studies have been performed to characterize changes in backbone and side chain dynamics in proteins upon ligand binding (*10*, *11*, *13*, *14*, *16*, *17*, *19*, *21*, *24*, *46*) while other investigations have focused on the backbone dynamics of peptide ligands (*47*−*49*).

A large body of spin relaxation data has been recorded to aid in the understanding of the relation between motion and binding in the case of the PLCC SH2 domain. Backbone ^{15}N and side chain ^{2}H rates have been measured for the free and bound states of the PLCC SH2 domain (*10*, *11*, *13*, *50*), supplemented in this study with relaxation data for the bound pY1021 peptide. Notably, ^{15}N relaxation data establish that nearly all of the backbone amides from residues that interact with the peptide are relatively well ordered in the free protein and exhibit no significant reduction in fast time scale dynamics in the bound state (*11*). In contrast, side chain dynamics are much more varied. ^{2}H spin relaxation data are consistent with a restriction of motion for the protein in the pTyr binding region upon addition of ligand, while methyls that contact residues C-terminal to the pTyr are very mobile in both apo and ligated states of the protein (for example, Leu βE4 C$\delta1$ and C$\delta2$ and Leu BG2 C$\delta1$) (*10*). In addition, side chains of Arg 37, 39, 50, and 59 that contact the pTyr of the peptide are broadened in NMR spectra, indicating millisecond time scale dynamics (*50*). The amplitudes of the fast time scale dynamics of the backbone amides in the pY1021 peptide are most restricted at I5, position +1, and increase toward the C-terminus (Figure 5a). Order parameters for D3−D10 average to 0.70, approximately 0.1 below average values for the protein. The dynamics of methyl-containing side chains in the peptide appear to be more extensive, not surprisingly, than motions of the backbone. Notably, the S^2_{axis} value for I5 $\delta1$ is higher than for I6 $\delta1$ or L8 $\delta1$,$\delta2$, consistent with previous observations that residues that contribute more to binding tend to be more static (*10*). However, five of the six methyl groups in the peptide (excluding I5 $\gamma2$) are dynamic, with order parameters that are either as low as or lower than one standard deviation from average values tabulated over a series of proteins. Most striking is the complementarity in dynamics of side chains that span the interface. A picture emerges of a dynamic complex, with interacting protein and peptide residues showing significant mobility. In this context, it is useful to think about an interface in which side chains are exchanging between conformers, with the dynamics serving to modulate the interaction between the ligand and protein. The potential relation between dynamics and affinity may be of particular importance to the PLCC SH2−pY1021 complex. It is clear, for example, that the binding energy has a strong component from electrostatics for SH2 domain peptide interactions in general. However, for the PLCC SH2 domain, this is particularly the case since four Arg residues line the binding pocket (*8*). In comparison, there are two for the Src SH2 domain (*6*). Thus, the combination of strong electrostatics and a static hydrophobic interface might decrease the dissociation rate of the PLCC complex to the point where biological function is compromised. In this regard, higher

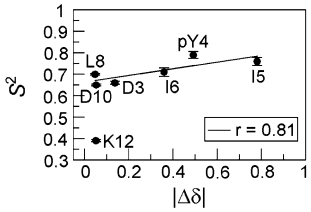

FIGURE 6: Backbone peptide amide order parameters squared (S^2) as a function of the absolute value of amide proton chemical shift differences in parts per million ($|\Delta\delta|$). $|\Delta\delta|$ corresponds to the difference in shifts in the free and bound states of the pY1021 peptide. The least-squares fit to the experimental data is shown as a solid line ($r = 0.81$, $P = 0.051$), excluding data for K12.

than average dynamics in this complex (at the level of both the protein and peptide) may serve to moderate the affinity somewhat, compensating for the charge interactions between the pTyr of the peptide and the (very) basic binding pocket.

Comparison with Other Systems. The ^{15}N relaxation properties of the bound pY1021 peptide are somewhat distinct from those measured for a 19-residue peptide derived from the smooth muscle myosin light chain kinase (smMLCKp) calmodulin-binding domain in complex with calmodulin (CaM) (*48*). Unlike the pY1021 peptide, the smMLCKp peptide exhibited little variation in ^{15}N relaxation along its length (S^2 values range from 0.79 to 0.86). The distinction in peptide dynamics likely reflects differences in the way that each peptide interacts with its target. For example, CaM binds the smMLCKp peptide with a very high affinity ($K_d \sim 1$ nM) and in a manner that largely buries the peptide. In contrast, the affinity of the PLCC SH2 domain for the pY1021 peptide is relatively modest (0.35 μM) and much of the bound peptide is solvent accessible (*8*). The dynamics of peptides in other complexes, for example, the 22-residue S-peptide bound to the S-protein [both derived from cleavage of ribonuclease A by subtilisin (*47*)], show trends that are similar to those reported here. Although the bound S-peptide has a much longer stretch of residues with high order parameters (S^2 values of >0.8 for 13 contiguous residues), the amplitude of fast time scale dynamics increases measurably toward the peptide termini where few residues interact with the S-protein. Thus, as illustrated by these examples, the mode of binding and the extent of interaction can have significant effects on the dynamic properties of small ligands.

Recently, Landry demonstrated a correlation between the free energy of binding and amide chemical shift perturbations for various pairings of wild-type and mutant DnaJ J-domain (Jd) and DnaK ATPase domain (Kase) proteins: those pairings that bind with higher affinity also show larger amide chemical shift perturbations for residues in the Jd domain (*51*). The author suggests that these results indicate that the complex is not static but exists as a dynamic ensemble of conformational states and that the more tightly interacting pairs have smaller conformational fluctuations in the bound state (biased toward a state with a larger chemical shift perturbation) than the more weakly interacting pairs.

Binding of the PLCC SH2 domain to mutated pY1021 peptides has not been investigated; however, it is still instructive to compare amide chemical shift changes in pY1021 upon binding PLCC with the dynamics of backbone amides in the bound pY1021 peptide (Figure 6). This comparison reveals a correlation between amide ^{15}N order parameters and amide ^{1}H chemical shift perturbations, with those residues exhibiting the largest chemical shift changes also among the most restricted dynamically in the complex.

Concluding Remarks. In a set of previous studies, the dynamics of both backbone and side chain methyl positions in apo and ligand bound states of the PLCC SH2 domain have been probed using ^{15}N and ^{2}H spin relaxation (*10*, *11*, *13*, *50*). Here, this work is supplemented by a study of the dynamics of a 12-residue phosphorylated peptide comprising the Tyr-1021 site in the β-platelet-derived growth factor receptor. These combined studies underscore the utility of dynamics experiments in examining conformational fluctuations about low-energy states represented in NMR or crystal structures. We have shown for the PLCC SH2 domain−pY1021 peptide complex that the interface is highly dynamic, with residues on both partners showing extensive mobility. This level of motion may be important for moderating the strength of the peptide−protein interaction. This work makes it clear that an understanding of the factors that contribute to binding requires not only high-resolution static structures but also site-specific information about how such structures change over time.

ACKNOWLEDGMENT

This project would not have been possible without the discovery by Kathleen Binns (1972−2003), in the laboratory of T. Pawson, that the EphA4 kinase efficiently phosphorylates the Y1021 peptide. We thank H. Lin for preparation of the Y1021 peptide, K. Binns and the laboratory of T. Pawson for the plasmid encoding the EphA4 kinase, V. Kanelis for useful comments on the manuscript, O. Millet for valuable discussions and for MATLAB scripts used for fitting relaxation parameters, and members of the Forman-Kay and Kay laboratories for valuable discussions.

SUPPORTING INFORMATION AVAILABLE

Figures showing the differences in methyl ^{13}C and ^{1}H chemical shifts and amide ^{15}N chemical shifts between unbound and SH2 domain-bound states of the pY1021 peptide and tables with the LS-2 fitting parameters for the analysis of ^{15}N S^2 and ^{2}H $S_{axis}{}^2$ values for the SH2 domain-bound state of the pY1021 peptide. This material is available free of charge via the Internet at http://pubs.acs.org.

REFERENCES

1. Pawson, T., and Schlessinger, J. (1993) SH2 and SH3 domains, *Curr. Biol. 3*, 434−442.
2. Cohen, G. B., Ren, R., and Baltimore, D. (1995) Modular binding domains in signal transduction proteins, *Cell 80*, 237−248.
3. Berridge, M. J. (1993) Inositol trisphosphate and calcium signalling, *Nature 361*, 315−325.
4. Eck, M. J., Shoelson, S. E., and Harrison, S. C. (1993) Recognition of a high-affinity phosphotyrosyl peptide by the Src homology-2 domain of p56lck, *Nature 362*, 87−91.
5. Lee, C. H., Kominos, D., Jacques, S., Margolis, B., Schlessinger, J., Shoelson, S. E., and Kuriyan, J. (1994) Crystal structures of peptide complexes of the amino-terminal SH2 domain of the Syp tyrosine phosphatase, *Structure 2*, 423−438.
6. Waksman, G., Shoelson, S. E., Pant, N., Cowburn, D., and Kuriyan, J. (1993) Binding of a high affinity phosphotyrosyl peptide to the Src SH2 domain: Crystal structures of the complexed and peptide-free forms, *Cell 72*, 779−790.
7. Hwang, P. M., Li, C., Morra, M., Lillywhite, J., Muhandiram, D. R., Gertler, F., Terhorst, C., Kay, L. E., Pawson, T., Forman-Kay, J. D., and Li, S. C. (2002) A "three-pronged" binding

mechanism for the SAP/SH2D1A SH2 domain: Structural basis and relevance to the XLP syndrome, *EMBO J. 21*, 314−323.
8. Pascal, S. M., Singer, A. U., Gish, G., Yamazaki, T., Shoelson, S. E., Pawson, T., Kay, L. E., and Forman-Kay, J. D. (1994) Nuclear magnetic resonance structure of an SH2 domain of phospholipase C-γ1 complexed with a high affinity binding peptide, *Cell 77*, 461−472.
9. Songyang, Z., Shoelson, S. E., Chaudhuri, M., Gish, G., Pawson, T., Haser, W. G., King, F., Roberts, T., Ratnofsky, S., Lechleider, R. J., et al. (1993) SH2 domains recognize specific phosphopeptide sequences, *Cell 72*, 767−778.
10. Kay, L. E., Muhandiram, D. R., Wolf, G., Shoelson, S. E., and Forman-Kay, J. D. (1998) Correlation between binding and dynamics at SH2 domain interfaces, *Nat. Struct. Biol. 5*, 156−163.
11. Farrow, N. A., Muhandiram, R., Singer, A. U., Pascal, S. M., Kay, C. M., Gish, G., Shoelson, S. E., Pawson, T., Forman-Kay, J. D., and Kay, L. E. (1994) Backbone dynamics of a free and phosphopeptide-complexed Src homology 2 domain studied by ^{15}N NMR relaxation, *Biochemistry 33*, 5984−6003.
12. Muhandiram, D. R., Yamazaki, T., Sykes, B., and Kay, L. E. (1995) Measurements of deuterium T1 and T1rho relaxation times in uniformly ^{13}C labeled proteins in solution, *J. Am. Chem. Soc. 117*, 11536−11544.
13. Kay, L. E., Muhandiram, D. R., Farrow, N. A., Aubin, Y., and Forman-Kay, J. D. (1996) Correlation between dynamics and high affinity binding in an SH2 domain interaction, *Biochemistry 35*, 361−368.
14. Finerty, P. J., Jr., Muhandiram, D. R., and Forman-Kay, J. D. (2002) Side Chain Dynamics of the SAP SH2 Domain Correlate with a Binding Hot Spot and a Region with Conformational Plasticity, *J. Mol. Biol. 322*, 605−620.
15. Gagne, S. M., Tsuda, S., Spyracopoulos, L., Kay, L. E., and Sykes, B. D. (1998) Backbone and methyl dynamics of the regulatory domain of troponin C: Anisotropic rotational diffusion and contribution of conformational entropy to calcium affinity, *J. Mol. Biol. 278*, 667−686.
16. Loh, A. P., Pawley, N., Nicholson, L. K., and Oswald, R. E. (2001) An increase in side chain entropy facilitates effector binding: NMR characterization of the side chain methyl group dynamics in Cdc42Hs, *Biochemistry 40*, 4590−4600.
17. Lee, A. L., Kinnear, S. A., and Wand, A. J. (2000) Redistribution and loss of side chain entropy upon formation of a calmodulin-peptide complex, *Nat. Struct. Biol. 7*, 72−77.
18. Stivers, J. T., Abeygunawardana, C., and Mildvan, A. S. (1996) ^{15}N NMR relaxation studies of free and inhibitor-bound 4-oxalocrotonate tautomerase: Backbone dynamics and entropy changes of an enzyme upon inhibitor binding, *Biochemistry 35*, 16036−16047.
19. Yu, L., Zhu, C. X., Tse-Dinh, Y. C., and Fesik, S. W. (1996) Backbone dynamics of the C-terminal domain of *Escherichia coli* topoisomerase I in the absence and presence of single-stranded DNA, *Biochemistry 35*, 9661−9666.
20. Nicholson, L. K., Kay, L. E., Baldisseri, D. M., Arango, J., Young, P. E., Bax, A., and Torchia, D. A. (1992) Dynamics of methyl groups in proteins as studied by proton-detected ^{13}C NMR spectroscopy. Application to the leucine residues of staphylococcal nuclease, *Biochemistry 31*, 5253−5263.
21. Zhang, W., Smithgall, T. E., and Gmeiner, W. H. (1998) Self-association and backbone dynamics of the hck SH2 domain in the free and phosphopeptide-complexed forms, *Biochemistry 37*, 7119−7126.
22. Zidek, L., Novotny, M. V., and Stone, M. J. (1999) Increased protein backbone conformational entropy upon hydrophobic ligand binding, *Nat. Struct. Biol. 6*, 1118−1121.
23. Mittermaier, A., Kay, L. E., and Forman-Kay, J. D. (1999) Analysis of deuterium relaxation-derived methyl axis order parameters and correlation with local structure, *J. Biomol. NMR 13*, 181−185.
24. Engen, J. R., Gmeiner, W. H., Smithgall, T. E., and Smith, D. L. (1999) Hydrogen exchange shows peptide binding stabilizes motions in Hck SH2, *Biochemistry 38*, 8926−8935.
25. Schumacher, T. N., Mayr, L. M., Minor, D. L., Jr., Milhollen, M. A., Burgess, M. W., and Kim, P. S. (1996) Identification of D-peptide ligands through mirror-image phage display, *Science 271*, 1854−1857.
26. Binns, K. L., Taylor, P. P., Sicheri, F., Pawson, T., and Holland, S. J. (2000) Phosphorylation of tyrosine residues in the kinase domain and juxtamembrane region regulates the biological and catalytic activities of Eph receptors, *Mol. Cell. Biol. 20*, 4791−4805.
27. Kanelis, V., Donaldson, L., Muhandiram, D. R., Rotin, D., Forman-Kay, J. D., and Kay, L. E. (2000) Sequential assignment of proline-rich regions in proteins: Application to modular binding domain complexes, *J. Biomol. NMR 16*, 253−259.
28. Kay, L. E. (1995) Pulsed field gradient multi-dimensional NMR methods for the study of protein structure and dynamics in solution, *Prog. Biophys. Mol. Biol. 63*, 277−299.
29. Sattler, M., Schleucher, J., and Griesinger, C. (1999) Heteronuclear multidimensional NMR experiments for the structure determination of proteins in solution employing pulsed field gradients, *Prog. NMR Spectrosc. 34*, 93−158.
30. Wüthrich, K. (1986) *NMR of Proteins and Nucleic Acids*, John Wiley and Sons, New York.
31. Johnson, B. A., and Blevins, R. A. (1994) NMRView: A computer program for the visualization and analysis of NMR data, *J. Biomol. NMR 4*, 603−614.
32. Akke, M., and Palmer, A. G. (1996) Monitoring macromolecular motions on microsecond-millisecond time scales by $R_{1\rho}$ and R_1 constant-relaxation-time NMR spectroscopy, *J. Am. Chem. Soc. 118*, 911−912.
33. Mulder, F. A., Mittermaier, A., Hon, B., Dahlquist, F. W., and Kay, L. E. (2001) Studying excited states of proteins by NMR spectroscopy, *Nat. Struct. Biol. 8*, 932−935.
34. Delaglio, F., Grzesiek, S., Vuister, G., Zhu, G., Pfeifer, J., and Bax, A. (1995) NMR Pipe: A multidimensional spectral processing system based on UNIX pipes, *J. Biomol. NMR 6*, 277−293.
35. Pintar, A., Hensmann, M., Jumel, K., Pitkeathly, M., Harding, S. E., and Campbell, I. D. (1996) Solution studies of the SH2 domain from the fyn tyrosine kinase: Secondary structure, backbone dynamics and protein association, *Eur. Biophys. J. 24*, 371−380.
36. Millet, O., Muhandiram, D. R., Skrynnikov, N. R., and Kay, L. E. (2002) Deuterium spin probes of side-chain dynamics in proteins. 1. Measurement of five relaxation rates per deuteron in ^{13}C-labeled and fractionally ^{2}H-enriched proteins in solution, *J. Am. Chem. Soc. 124*, 6439−6448.
37. Skrynnikov, N. R., Millet, O., and Kay, L. E. (2002) Deuterium spin probes of side-chain dynamics in proteins. 2. Spectral density mapping and identification of nanosecond time-scale side-chain motions, *J. Am. Chem. Soc. 124*, 6449−6460.
38. Jacobsen, J. P., Bildsoe, H. K., and Schaumburg, K. (1976) Application of density of matrix formalism in NMR spectroscopy. II. The one-spin-1 case in anisotropic phase, *J. Magn. Reson. 23*, 153−164.
39. Valeur, B., Jarry, J.-P., Geny, F., and Monnerie, L. (1975) Dynamics of Macromolecular Chains. II. Orientation Relaxation Generated by Elementary Three-Bond Motions and Notion of an Independent Kinetic Segment, *J. Polym. Sci., Part B: Polym. Phys. 13*, 675−682.
40. Lipari, G., and Szabo, A. (1982) Model-Free Approach to the Interpretation of Nuclear Magnetic Resonance Relaxation of Macromoluecules: 1. Theory and Range of Validity, *J. Am. Chem. Soc. 104*, 4546−4559.
41. Lipari, G., and Szabo, A. (1982) Model-Free Approach to the Interpretation of Nuclear Magnetic Resonance Relaxation of Macromoluecules: 2. Analysis of Experimental Results, *J. Am. Chem. Soc. 104*, 4559−4570.
42. Kay, L. E., Torchia, D. A., and Bax, A. (1989) Backbone dynamics of proteins as studied by ^{15}N inverse detected heteronuclear NMR spectroscopy: Application to staphylococcal nuclease, *Biochemistry 28*, 8972−8979.
43. Clore, G. M., Driscoll, P. C., Wingfield, P. T., and Gronenborn, A. M. (1990) Analysis of the backbone dynamics of interleukin-1β using two-dimensional inverse detected heteronuclear ^{15}N−^{1}H NMR spectroscopy, *Biochemistry 29*, 7387−7401.
44. Conte, L. L., Chothia, C., and Janin, J. (1999) The atomic structure of protein−protein recognition sites, *J. Mol. Biol. 285*, 2177−2198.
45. Palmer, A. G., III, Kroenke, C. D., and Loria, J. P. (2001) Nuclear magnetic resonance methods for quantifying microsecond-to-millisecond motions in biological macromolecules, *Methods Enzymol. 339*, 204−238.
46. Kristensen, S. M., Siegal, G., Sankar, A., and Driscoll, P. C. (2000) Backbone dynamics of the C-terminal SH2 domain of the p85α subunit of phosphoinositide 3-kinase: Effect of phosphotyrosine-peptide binding and characterization of slow conformational exchange processes, *J. Mol. Biol. 299*, 771−788.

47. Alexandrescu, A. T., Rathgeb-Szabo, K., Rumpel, K., Jahnke, W., Schulthess, T., and Kammerer, R. A. (1998) ^{15}N backbone dynamics of the S-peptide from ribonuclease A in its free and S-protein bound forms: Toward a site-specific analysis of entropy changes upon folding, *Protein Sci. 7*, 389−402.
48. Chen, C., Feng, Y., Short, J. H., and Wand, A. J. (1993) The main chain dynamics of a peptide bound to calmodulin, *Arch. Biochem. Biophys. 306*, 510−514.
49. Gizachew, D., and Oswald, R. E. (2001) Concerted motion of a protein-peptide complex: Backbone dynamics studies of an ^{15}N-labeled peptide derived from P_{21}-activated kinase bound to Cdc42Hs·GMPPCP, *Biochemistry 40*, 14368−14375.
50. Pascal, S. M., Yamazaki, T., Singer, A. U., Kay, L. E., and Forman-Kay, J. D. (1995) Structural and dynamic characterization of the phosphotyrosine binding region of a Src homology 2 domain−phosphopeptide complex by NMR relaxation, proton exchange, and chemical shift approaches, *Biochemistry 34*, 11353−11362.
51. Landry, S. J. (2003) Structure and Energetics of an Allele-Specific Genetic Interaction between dnaJ and dnaK: Correlation of Nuclear Magnetic Resonance Chemical Shift Perturbations in the J-Domain of Hsp40/DnaJ with Binding Affinity for the ATPase Domain of Hsp70/DnaK, *Biochemistry 42*, 4926−4936.
52. Koradi, R., Billeter, M., and Wuthrich, K. (1996) MOLMOL: A program for display and analysis of macromolecular structures, *J. Mol. Graphics 14*, 29−32 and 51−55.
53. Singer, A. U. (1998) Solution Structure and Electrostatic Properties of an SH2 Domain/Phosphopeptide Complex, Ph.D. Thesis in Medical and Molecular Genetics, University of Toronto, Toronto.

BI048641K